Title	CHD1L promotes hepatocellular carcinoma progression and metastasis in mice and is associated with these processes in human patients
Author(s)	Chen, L; Chan, THM; Yuan, YF; Hu, L; Huang, J; Ma, S; Wang, J; Dong, SS; Tang, KH; Xie, D; Li, Y; Guan, XY
Citation	Journal Of Clinical Investigation, 2010, v. 120 n. 4, p. 1178-1191
Issued Date	2010
URL	http://hdl.handle.net/10722/71912
Rights	Creative Commons: Attribution 3.0 Hong Kong License

 Related Commentary, page 1031

CHD1L promotes hepatocellular carcinoma progression and metastasis in mice and is associated with these processes in human patients

Leilei Chen,[1] Tim Hon Man Chan,[1] Yun-Fei Yuan,[2] Liang Hu,[1] Jun Huang,[2] Stephanie Ma,[3] Jian Wang,[1] Sui-Sui Dong,[1] Kwan Ho Tang,[3] Dan Xie,[4] Yan Li,[4] and Xin-Yuan Guan[1,4]

[1]Department of Clinical Oncology, University of Hong Kong, China. [2]Department of Hepatobiliary Oncology, Sun Yat-sen University Cancer Center, Guangzhou, China. [3]Department of Pathology, University of Hong Kong. [4]State Key Laboratory of Oncology in Southern China, Cancer Center, Sun Yat-sen University Cancer Center.

Chromodomain helicase/ATPase DNA binding protein 1–like gene (*CHD1L*) is a recently identified oncogene localized at 1q21, a frequently amplified region in hepatocellular carcinoma (HCC). To explore its oncogenic mechanisms, we set out to identify CHD1L-regulated genes using a chromatin immunoprecipitation–based (ChIP-based) cloning strategy in a human HCC cell line. We then further characterized 1 identified gene, *ARHGEF9*, which encodes a specific guanine nucleotide exchange factor (GEF) for the Rho small GTPase Cdc42. Overexpression of ARHGEF9 was detected in approximately half the human HCC samples analyzed and positively correlated with CHD1L overexpression. In vitro and in vivo functional studies in mice showed that CHD1L contributed to tumor cell migration, invasion, and metastasis by increasing cell motility and inducing filopodia formation and epithelial-mesenchymal transition (EMT) via ARHGEF9-mediated Cdc42 activation. Silencing ARHGEF9 expression by RNAi effectively abolished the invasive and metastatic abilities of CHD1L in mice. Furthermore, investigation of clinical HCC specimens showed that CHD1L and ARHGEF9 were markedly overexpressed in metastatic HCC tissue compared with healthy tissue. Increased expression of CHD1L was often observed at the invasive front of HCC tumors and correlated with venous infiltration, microsatellite tumor nodule formation, and poor disease-free survival. These findings suggest that CHD1L-ARHGEF9-Cdc42-EMT might be a novel pathway involved in HCC progression and metastasis.

Introduction

Hepatocellular carcinoma (HCC) is ranked as the fifth most frequent cancer in the world and affects 1 million people annually (1). The prognosis of HCC is very poor, and the 5-year survival rate worldwide is less than 5%, mainly because of a high potential for vascular invasion, metastasis, and recurrence even after surgical resection (2). Like other cancers, HCC metastasis is a multistep process that includes tumor cells' invasion of tumor cells into the surrounding tissues, entry of tumor cells into the systemic circulation (intravasation), their survival in circulation, extravasation of the cells to distant organs, and finally the formation of secondary tumors (3). Genetically, the loss of alleles on 16q and 8p has been associated with HCC metastasis (4, 5). Recently, several genes associated with HCC metastasis have been identified, including *cortactin* (6), *CLU* (7), *HTPAP* (8), *Twist* (9), and *Pyk2* (10).

Amplification of 1q21 is one of the most frequent genetic alterations in HCC (11–13) and has been associated with HCC metastasis (14). Recently, 1 candidate oncogene, chromodomain helicase/ATPase DNA binding protein 1–like gene (*CHD1L*; also known as *ALC1*), has been isolated from the 1q21 amplicon (15). Our previous studies have demonstrated that *CHD1L* is frequently amplified and overexpressed in HCCs and plays an important role in the development of HCC (15, 16). CHD1L belongs to SNF2-like subfamily of the sucrose nonfermenting 2 (Snf2) family. Each SNF2-like protein contains a domain (approximately 400 amino acids) with highly conserved helicase motifs (17). Most SNF2-like proteins participate in various nuclear activities, including transcriptional activation or repression, DNA repair, and recombination (18, 19). These findings prompted us to investigate whether CHD1L protein functions as a transcriptional regulator and to identify genes potentially regulated by CHD1L.

To identify genes potentially regulated by CHD1L, CHD1L DNA-binding sequences were isolated using a chromatin immunoprecipitation–based (ChIP-based) cloning strategy (20). Using this strategy, 35 CHD1L-binding loci were isolated, and genes near these loci were identified by BLAST searches. Of the CHD1L-regulated genes, *ARHGEF9* was particularly interesting, as it is able to activate the Rho small GTPase Cdc42. One of the important molecular mechanisms in cancer metastasis is the activation of the Rho family of small GTPases, which in turn leads to the rearrangement of the actin cytoskeleton and modulates cadherin-dependent cell-cell contacts (21–23). In the present study, overexpression of ARHGEF9 was observed in 51.4% of primary HCC cases and was positively correlated with CHD1L expression, which suggests that expression of ARHGEF9 is regulated by CHD1L. Furthermore, as detected by functional studies, upregulation of ARHGEF9 by CHD1L increased the Cdc42-GTP level in HCC cells, induced HCC invasion and metastasis through the relocalization of actin to filopodia-like

Conflict of interest: The authors have declared that no conflict of interest exists.
Citation for this article: *J Clin Invest.* 2010;120(4):1178–1191. doi:10.1172/JCI40665.

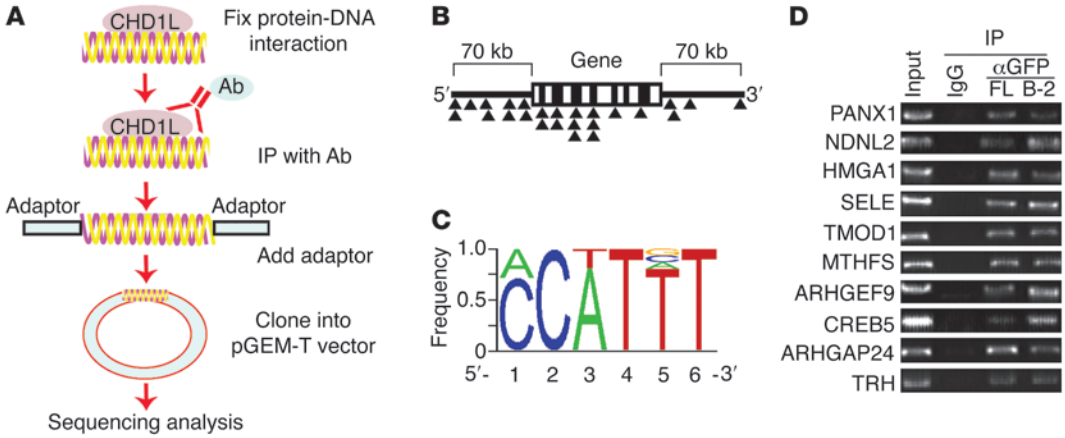

Figure 1

Identification of CHD1L target genes and the putative CHD1L-binding motif. (**A**) Genome-wide mapping of CHD1L target genes using a modified ChIP-based cloning approach. Cultured cells were treated with formaldehyde to crosslink protein-DNA complexes. A specific antibody was used to capture CHD1L-bound DNA sequences by immunoprecipitation. The precipitated DNA fragments were ligated to an adaptor, cloned into the pGEM-T vector, and analyzed by sequencing. (**B**) Distribution of CHD1L-binding loci, indicated by triangles. (**C**) Top-scoring motif identified in an unbiased analysis of CHD1L target genes using MatInspector software. The height of each letter is proportional to its frequency. (**D**) Confirmation of 10 randomly selected CHD1L target genes by ChIP-PCR using anti-GFP antibodies FL and B-2 or pooled IgG from mouse and rabbit (negative control) in GFP/CHD1L-7703-C3 cells. Input represents amplification of a 1:50 dilution of total input chromatin.

structures, and promoted the epithelial-mesenchymal transition (EMT). The clinical significance of CHD1L overexpression was also addressed in this study.

Results

Identification of CHD1L target genes. Like other SNF2-like family members, CHD1L may also be able to regulate gene expression at the transcriptional level. To identify genes potentially regulated by CHD1L, CHD1L target genes were isolated using a modified ChIP-based cloning strategy (Figure 1A). Briefly, the *CHD1L* gene was cloned into expressing vector tagged with GFP and stably transfected into the HCC cell line QGY-7703, in which endogenous expression of CHD1L is extremely low (15, 16). We selected 2 GFP/CHD1L transfectants (GFP/CHD1L-7703-C3 and -C6) with high expression of the GFP/CHD1L fusion protein and 2 GFP empty vector transfectants (GFP-7703-C3 and -C4) for further study (Supplemental Figure 1A; supplemental material available online with this article; doi:10.1172/JCI40665DS1). Using the strategy outlined in Figure 1A, 35 clones were isolated and sequenced. To exclude the contamination of GFP-bound DNA fragments, a parallel experiment was performed using GFP transfectants (GFP-7703-C3 and -C4), from which no clones were obtained.

A BLAST search was used to identify genes near the potential CHD1L-binding sites. Among the 35 CHD1L-binding loci, 25 of 35 (71.4%) CHD1L binding sites were mapped less than 70 kb away from known genes; we classified these as 5′ (9 loci), introns (12 loci), or 3′ (4 loci; Figure 1B and Supplemental Table 1). All 35 DNA sequences (mean length, 325 bp) were analyzed by MatInspector software (Genomatrix) to search for potential CHD1L-binding motifs (24). An 11-bp SWI/SNF-related DNA-binding motif was detected in 17 of 35 (48.6%) CHD1L-binding sequences (Supplemental Table 2). The motif contained a hexameric core sequence of C/A-C-A/T-T-T-T (Figure 1C) and was similar to a known SWI/SNF-related, matrix-associated, actin-dependent regulator of chromatin, subfamily a, member 3 (SMARCA3; also named SNF2-like 3) motif (25). To confirm the CHD1L-binding sites, we used PCR to detect 10 CHD1L-binding sites with the CHD1L-binding motif in the ChIP-isolated CHD1L-bound DNA fragments using 2 different GFP antibodies, FL and B-2. As expected, the amplified DNA fragments were detected in ChIP-isolated DNA, but not in controls (Figure 1D). These data indicate that CHD1L may transcriptionally regulate target genes by binding to a specific DNA-binding motif.

CHD1L upregulates ARHGEF9 expression. The CHD1L-regulated gene *ARHGEF9* was further characterized because of its ability to activate the Rho small GTPase Cdc42, which may play a key role in tumor metastasis. To confirm that CHD1L protein binds to *ARHGEF9*, EMSA was performed using an oligonucleotide probe from the *ARHGEF9* locus (CHD1L_57; Supplemental Figure 1B). CHD1L specifically bound to the digoxigenin-labeled (DIG-labeled) probe (Figure 2A). To determine whether the expression of ARHGEF9 was modulated in a CHD1L-dependent manner, the *CHD1L* gene was transiently transfected into the HCC cell line QGY-7703 and into immortalized liver cell line LO-2, and the effect of ectopic expression of CHD1L on ARHGEF9 expression was tested by quantitative real-time PCR (qPCR). As shown in Figure 2B, ARHGEF9 expression was upregulated by CHD1L. Furthermore, decreased expression of ARHGEF9 was detected when CHD1L expression was silenced in the HCC cell line PLC8024 by RNAi with an siRNA against CHD1L (siCHD1L), but not with an siRNA against GAPDH (siGAPDH; Figure 2C).

CHD1L activates Cdc42 through ARHGEF9 upregulation. As ARHGEF9 is a guanine nucleotide exchange factor (GEF) specific for Cdc42 (26), we investigated whether CHD1L could activate Cdc42 through the upregulation of ARHGEF9 in HCC cells. For this purpose, *CHD1L* was stably transfected into QGY-7703 and LO-2 cells (referred to herein as CHD1L-7703 and CHD1L-LO2, respectively), and empty vector was used as a control (referred to as Vec-7703 and Vec-LO2). Ectopic expression of CHD1L upregulated ARHGEF9 expression, which subsequently activated

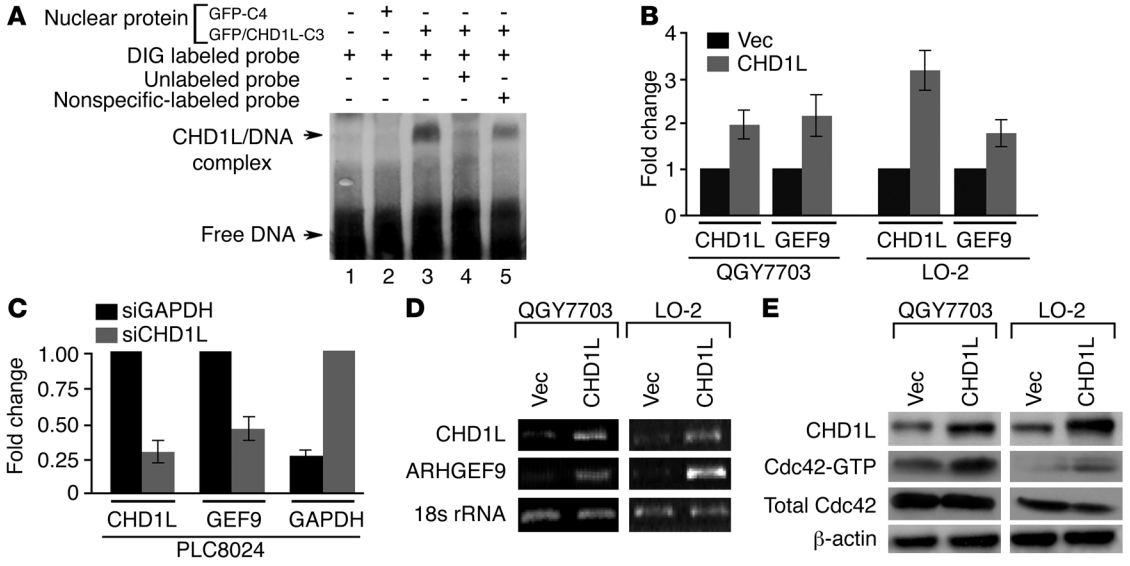

Figure 2

ARHGEF9 is a validated target gene of CHD1L and induces Cdc42 activation. (**A**) EMSA was used to detect the interaction between CHD1L and ARHGEF9 double-stranded DNA probes. Lane 1, without NE; lane 2, with NE from GFP-7703-C4 cells and DIG-labeled probe; lane 3, with NE from GFP/CHD1L-7703-C3 cells and labeled probe; lane 4, same as lane 3 plus a 50-fold molar excess of unlabeled probe; lane 5, same as lane 3 plus excess unlabeled nonspecific probe. (**B**) ARHGEF9 expression was modulated by CHD1L. After transient transfection, relative expression of CHD1L and ARHGEF9 was detected in Vec-7703, CHD1L-7703, Vec-LO2, and CHD1L-LO2 cells by qPCR. 18S rRNA was used as an internal control. (**C**) Silencing CHD1L expression downregulated ARHGEF9 expression. PLC8024 cells were treated with siCHD1L or siGAPDH as a negative control. The fold changes in CHD1L, ARHGEF9, and GAPDH expression in siCHD1L- or siGAPDH-treated PLC8024 cells were detected by qPCR. (**D**) Compared with empty vector transfectants, ARHGEF9 expression was upregulated in QGY-7703 and LO-2 cells stably expressing CHD1L, as detected by RT-PCR. 18S rRNA was used an endogenous control. (**E**) Expression of CHD1L, Cdc42-GTP, and total Cdc42, detected by Western blot. Cdc42-GTP increased in CHD1L-7703 and CHD1L-LO2 cells. β-Actin was used as a loading control.

Cdc42 (Figure 2D). As shown in Figure 2E, increased Cdc42-GTP, the active form of Cdc42, was detected in both CHD1L-7703 and CHD1L-LO2 cells compared with Vec-7703 and Vec-LO2 cells. These results suggested that CHD1L could active Cdc42 by the upregulation of ARHGEF9.

CHD1L induces filopodia formation and EMT. We next investigated whether CHD1L overexpression affects the actin cytoskeleton in HCC cell lines, because Cdc42 can promote actin filament assembly and filopodia formation (27). First, we found that the cell morphology of CHD1L-LO2 and CHD1L-7703 cells changed from an epithelial-like to a fibroblastic-like morphology (Figure 3A), which suggests that these cells underwent a rearrangement of the cytoskeleton. F-actin staining showed that filopodia formation dramatically increased in CHD1L-7703 cells, suggestive of substantial relocalization of actin to filopodia in these cells (Figure 3B).

Since rearrangement of the actin cytoskeleton is often regarded as a signature of the EMT, the effect of CHD1L on the EMT was investigated. The expression of 3 tested epithelial markers (E-cadherin, α-catenin, and β-catenin) decreased, while the expression of 4 tested mesenchymal markers (N-cadherin, vimentin, fibronectin, and α-SMA) increased, in CHD1L-expressing cells compared with empty vector–transfected cells (Figure 3C). Because the downregulation of E-cadherin has been closely associated with EMT, and loss of E-cadherin leads to the accumulation of β-catenin in the cytoplasm and/or nucleus (28), double immunofluorescence (IF) staining of E-cadherin and β-catenin was performed in Vec-7703 and CHD1L-7703 cells to further investigate the effect of CHD1L on the E-cadherin/β-catenin complex. Membranous expression of both E-cadherin and β-catenin decreased in CHD1L-7703 cells compared with Vec-7703 cells; however, no obvious accumulation of β-catenin in the nucleus was observed (Figure 3D). IF staining also confirmed increased expression of the mesenchymal markers fibronectin and vimentin in CHD1L-7703 cells compared with Vec-7703 cells (Figure 3E). All these results demonstrated that CHD1L-7703 cells underwent EMT.

CHD1L increases cell motility and invasion. The EMT promotes tumor progression by increasing the invasiveness and migratory capacity of the tumor cell. To test whether CHD1L-7703 and CHD1L-LO2 cells acquired greater migratory and invasive capabilities, an in vitro scratch wound healing assay and a Matrigel invasion assay were performed. The wound healing assay demonstrated that the ectopic expression of CHD1L increased cell motility in both CHD1L-7703 and CHD1L-LO2 cells compared with Vec-7703 and Vec-LO2 cells (Figure 3F). Similarly, the Matrigel invasion assay showed that the invasiveness of the CHD1L-expressing cells was significantly higher than empty vector–transfected cells ($P < 0.001$, independent Student's t test; Supplemental Figure 2 and Figure 3G).

ARHGEF9 is responsible for CHD1L-induced Cdc42 activation. To investigate whether activation of Cdc42 by ARHGEF9 is responsible for CHD1L-induced filopodia formation, EMT, and tumor invasion, RNAi was used to silence ARHGEF9 expression. CHD1L-7703 cells were treated with siRNAs against ARHGEF9 (siARHGEF9-1 or siARHGEF9-2) or siGAPDH as a negative control. After siRNA treatment, the expression of ARHGEF9 was dramatically decreased (Supplemental Figure 3A), which resulted

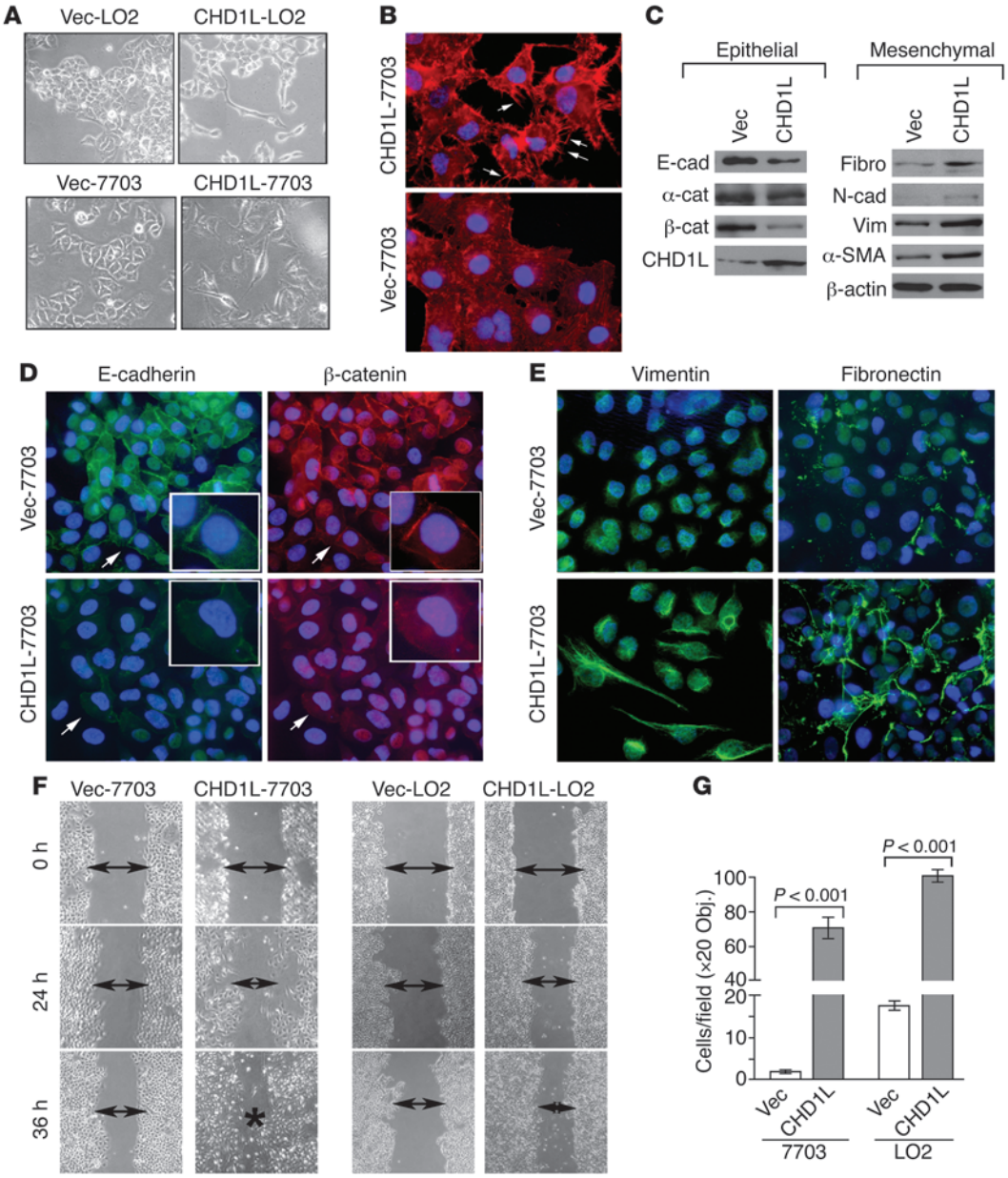

Figure 3

CHD1L induces filopodia formation, EMT, and cell migration and invasion. (**A**) Representative images of cell morphology in Vec-LO2, CHD1L-LO2, Vec-7703, and CHD1L-7703 cells. (**B**) Redistribution of actin filaments to filopodia-like structures in CHD1L-7703 cells (arrows). The cells were stained for F-actin and counterstained with DAPI to visualize the nuclei. (**C**) Expression of epithelial markers (E-cadherin, α-catenin, and β-catenin) and mesenchymal markers (fibronectin, N-cadherin, vimentin, and α-SMA), compared between Vec-7703 and CHD1L-7703 cells by Western blot. (**D**) Double IF staining of E-cadherin and β-catenin was performed in Vec-7703 and CHD1L-7703 cells. Arrows denote the regions shown at higher magnification in the insets. (**E**) Fibronectin and vimentin in Vec-7703 and CHD1L-7703 cells were compared by IF staining; nuclei were counterstained with DAPI. (**F**) Cell migration rates of Vec-7703, CHD1L-7703, Vec-LO2, and CHD1L-LO2 cells were compared via wound healing assays. Microscopic observation was recorded at 0, 24, and 36 hours after scratching the surface of a confluent layer of cells. (**G**) Invasion rates of Vec-7703, CHD1L-7703, Vec-LO2, and CHD1L-LO2 cells. Number of cells that invaded through the Matrigel was counted in 10 fields under the ×20 objective lens. Original magnification, ×200 (**A**); ×400 (**B**, **D**, and **E**); ×1,000 (**D**, insets); ×100 (**F**).

in the reduced expression of Cdc42-GTP (Figure 4A). CHD1L-induced EMT was also blocked by ARHGEF9 siRNA treatment, as evidenced by the increased E-cadherin and decreased vimentin expression as well as by the decreased CHD1L-mediated filopodia formation (Figure 4, A and B). More importantly, CHD1L-7703 cells lost their invasive ability after the ARHGEF9 siRNA treatment. Matrigel invasion assay showed that cell invasion significantly decreased in siARHGEF9-1– and siARHGEF9-2–treated compared with siGAPDH-treated or untreated CHD1L-7703 cells ($P < 0.001$, independent Student's t test; Figure 4C and Supple-

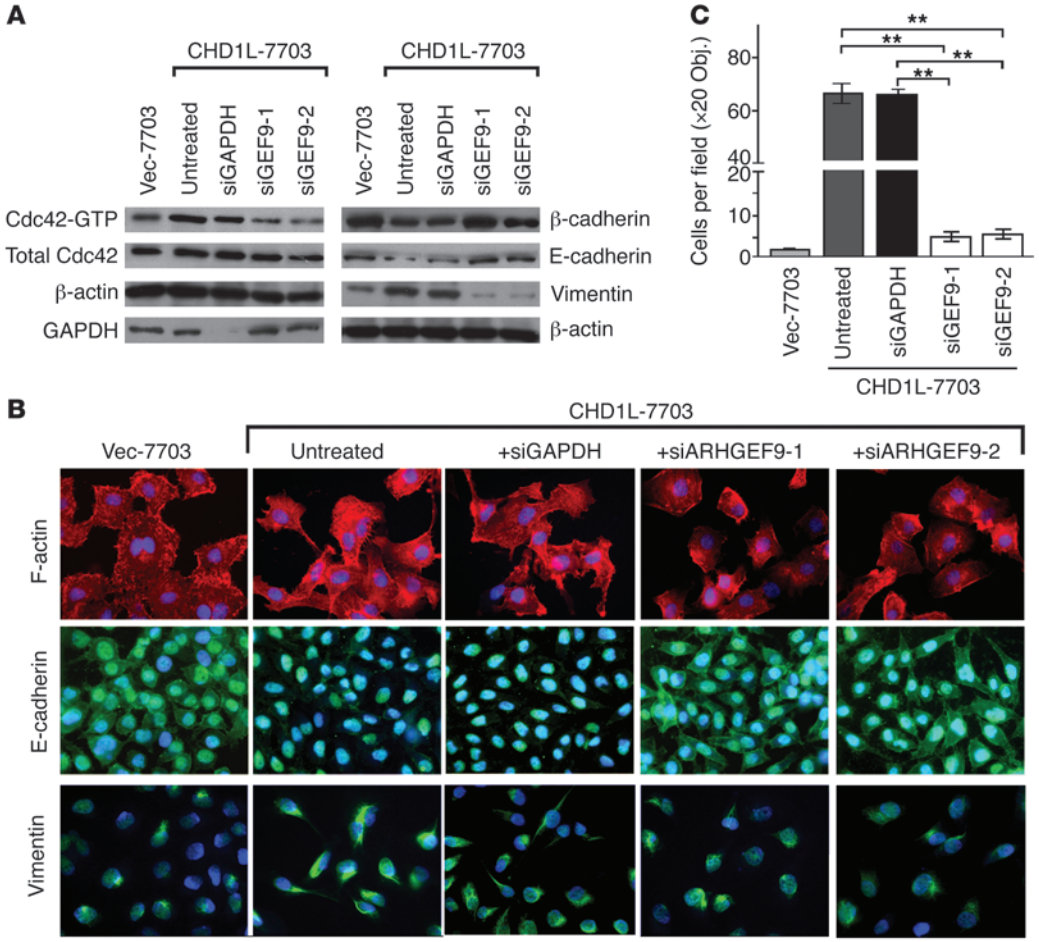

Figure 4

ARHGEF9 is responsible for CHD1L-induced Cdc42 activation, filopodia formation, EMT, and tumor cell migration and invasion. (**A**) After silencing ARHGEF9 expression in CHD1L-7703 cells after treatment with siARHGEF9-1 or siARHGEF9-2, expression of Cdc42-GTP and vimentin decreased, whereas expression of E-cadherin and β-catenin increased, relative to untreated or siGAPDH-treated cells. β-actin was used as a loading control. (**B**) Staining for F-actin demonstrated that filopodia formation in siARHGEF9-treated cells dramatically decreased compared with siGAPDH-treated cells. IF staining showed increased expression of E-cadherin (green) and decreased expression of vimentin (green) in CHD1L-7703 cells treated with siARHGEF9-1 or siARHGEF9-2 compared with untreated or siGAPDH-treated cells. Original magnification, ×400. (**C**) Invasive ability was inhibited in CHDL1-7703 cells treated with siARHGEF9-1 and siARHGEF9-2, detected by Matrigel invasion assays. Number of cells that invaded through the Matrigel was counted in 10 fields under the ×20 objective lens. $^{**}P < 0.001$, independent Student's *t* test.

mental Figure 3B). All these data suggest that CHD1L-induced filopodia formation, EMT, and tumor invasion are associated with ARHGEF9-induced activation of Cdc42 in HCC cells.

CHD1L promotes tumor metastasis in SCID mice. To investigate the in vivo effects of CHD1L overexpression on metastasis, an experimental metastasis assay was used to compare the metastatic nodules formed in the lungs and livers of SCID mice after inoculation with CHD1L-expressing or empty vector–transfected cells. At 8 weeks after injection, the mice were euthanized, and the lungs and livers were harvested. The number of metastatic nodules on the surface of the liver was significantly higher in mice injected with CHD1L-7703 cells than in mice injected with Vec-7703 cells (56 ± 17 versus 6.7 ± 5.6; $P < 0.001$, independent Student's *t* test; Figure 5A). Similarly, the number of metastatic nodules on the surface of the lungs was significantly higher in mice injected with CHD1L-7703 cells than in mice injected with Vec-7703 cells (17.8 ± 7.7 versus 3.5 ± 4.4; $P < 0.05$, independent Student's *t* test; Figure 5B). Histological studies confirmed that the lesions were caused by extravasation and subsequent tumor growth of CHD1L-transfected HCC cells into the lungs and livers (Figure 5, C and D).

CHD1L promotes invasion and metastasis via EMT. To further elucidate the invasive function of CHD1L in vivo, we examined whether HCC cell lines with a high expression of CHD1L undergo EMT during tumor progression. For this purpose, Vec-7703 and CHD1L-7703 cells, or Vec-LO2 and CHD1L-LO2 cells, were subcutaneously injected into the dorsal flanks of nude mice ($n = 5$ per group). Consistent with our previous study (15), tumor formation was observed in 4 of 5 and 1 of 5 CHD1L-7703– and Vec-7703–injected nude mice, respectively, and in 5 of 5 and 1 of 5 CHD1L-LO2– and Vec-LO2–injected nude mice, respectively (Figure 6A and Supplemental Table 3). A clear boundary between the tumor and its adjacent nontumor tissue was often observed in Vec-7703– or Vec-LO2–generated tumors; however, irregular

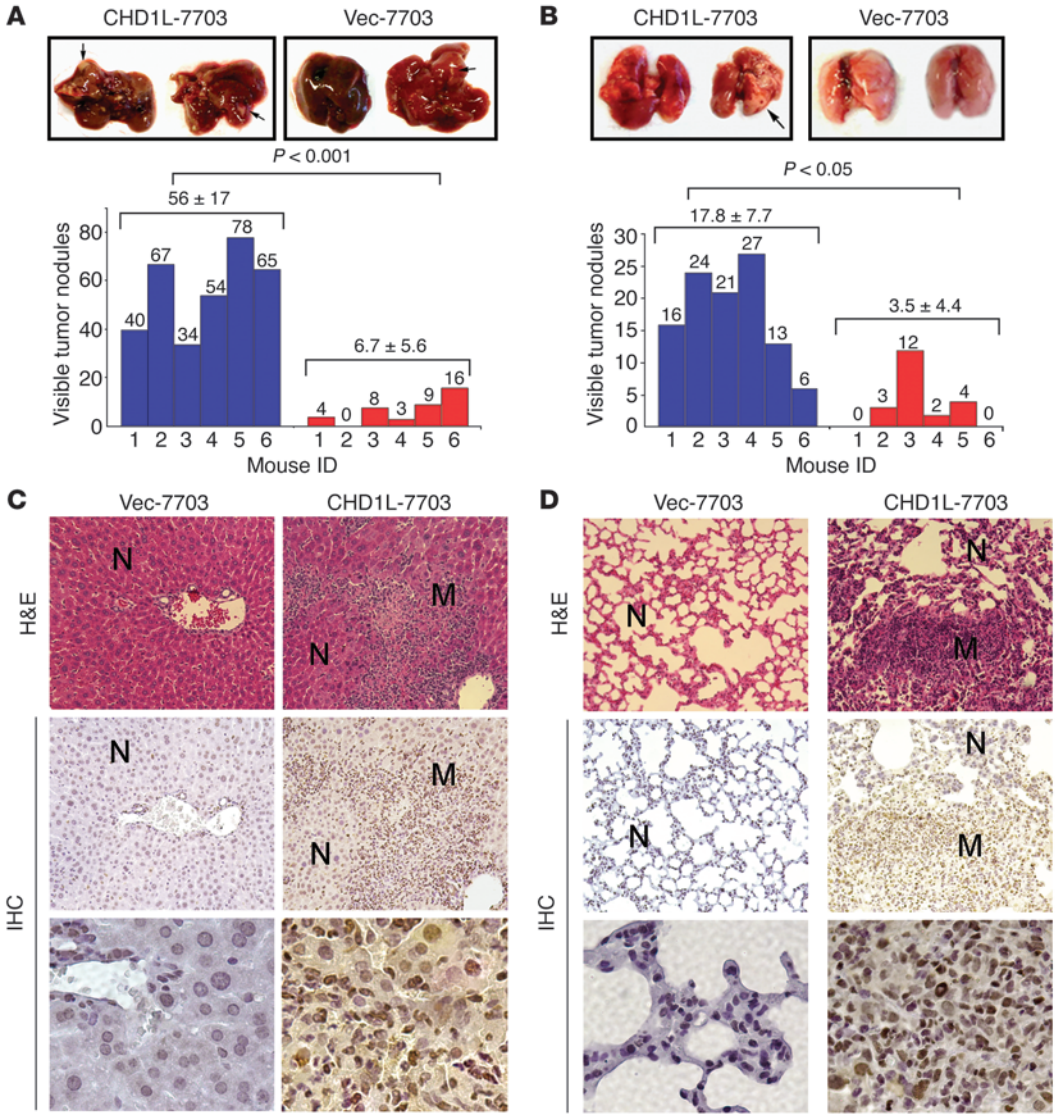

Figure 5

CHD1L promotes tumor metastasis in vivo. (**A** and **B**) Metastatic nodules (arrows) on the surface of the liver (**A**) and lung (**B**). Below, the number of nodules were quantified on livers and lungs of SCID mice ($n = 6$ per group) 8 weeks after tail vein injection of Vec-7703 (red bars) and CHD1L-7703 (blue bars) cells. Values for individual mice are shown above the bars; values by group are also denoted. (**C** and **D**) H&E staining and IHC staining with an anti-CHD1L antibody were performed on serial sections of metastatic tumors (M) and normal (N) liver (**C**) and lung (**D**). Original magnification, ×200 (top and middle rows); ×400 (bottom row).

tumor invasion was frequently observed in tumors induced by CHD1L-7703 or CHD1L-LO2 cells (Figure 6B, top). Furthermore, tumor microsatellite formations were observed near tumors in 2 of 4 and 3 of 5 CHD1L-7703– and CHD1L-LO2–derived tumors, respectively (Figure 6C, top). Immunohistochemical staining (IHC) with an anti-CHD1L antibody confirmed the expression of CHD1L in CHD1L-LO2– and CHD1L-7703–generated tumors (Figure 6, B and C, bottom).

To determine whether the EMT plays a role in tumor metastasis induced by CHD1L transfectants in the nude mouse, IHC with antibodies against E-cadherin and vimentin was performed on serial sections of each tumor. Decreased expression of E-cadherin and increased expression of vimentin was observed in tumors induced by CHD1L-LO2 or CHD1L-7703 cells compared with tumors induced by Vec-LO2 or Vec-7703 cells (Figure 6D). This suggests that the EMT promoted by CHD1L may play a key role in HCC invasion and metastasis.

CHD1L depletion reverses the invasive process of HCC cells and tumorigenesis in nude mice. We then examined whether CHD1L is required for the invasive and tumorigenic phenotypes of HCC cells by expressing shRNA to knock down CHD1L expression. We stably expressed shRNA from 2 different *CHD1L* sequences (shRNA1 and shRNA2) in the HCC cell line PLC8024 (referred to herein as shCHD1L-1–8024 and shCHD1L-2–8024 cells). Compared with PLC8024 cells expressing a control shRNA whose sequence did not match any known human gene (Con-8024 cells), expression of CHD1L dramatically decreased in shCHD1L-1–8024 and shCHD1L-2–8024 cells, as detected by qPCR and Western blot analysis (Figure 7,

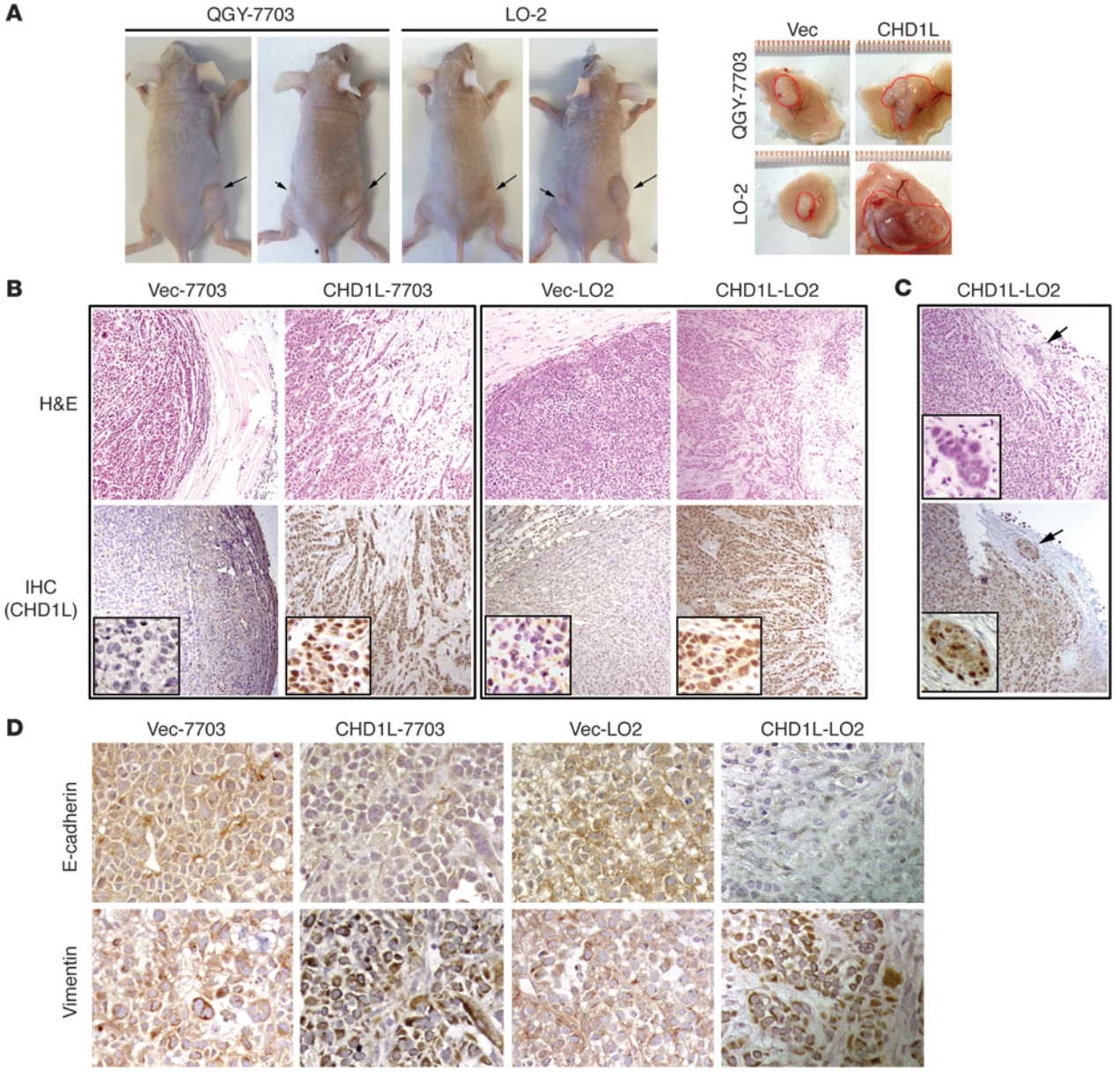

Figure 6

CHD1L promotes tumor invasion and metastasis in nude mice through the EMT. (**A**) Representative images of the tumors (arrows) formed in nude mice induced by vector-transfected cells (left dorsal flank) and CHD1L-expressing cells (right dorsal flank). Red outlines denote the tumor mass (**A**, right). (**B**) Tumors induced by vector-transfected cells had a clear boundary between the tumor and adjacent nontumor tissue, as detected by H&E staining. However, tumors induced by CHD1L-expressing cells displayed irregular invasive fronts. CHD1L expression was examined by IHC with an anti-CHD1L antibody in CHD1L-7703– or CHD1L-LO2–derived tumors and their control counterparts. Higher-magnification views are shown in the insets. (**C**) Representative microsatellite tumor formation was observed in the tumors induced by CHD1L-LO2 cells. Arrows denote the regions shown at higher magnification in the insets. (**D**) IHC staining for E-cadherin and vimentin on serial sections of tumors induced by Vec-7703, CHD1L-7702, Vec-LO2, and CHD1L-LO2 cells. Original magnification, ×100 (**B** and **C**); ×400 (**B** and **C**, insets, and **D**).

A and C). Moreover, CHD1L knockdown in shCHD1L-1–8024 and shCHD1L-2–8024 cells decreased the expression of *ARHGEF9* and Cdc42-GTP, which in turn led to decreased formation of filopodia, upregulation of E-cadherin, and downregulation of vimentin, finally reducing the cells' invasive ability (Figure 7, A–E). We next subcutaneously injected pooled shCHD1L-1–8024 and shCHD1L-2–8024 (referred to as shCHD1L-8024) and Con-8024 cells into nude mice. In contrast to Con-8024 cells (all 6 of which formed large tumors within 6 weeks), the mice injected with shCHD1L-8024 cells displayed either no tumor (4 of 6) or greatly reduced tumor growth (2 of 6; Figure 7F). The mean volume of tumors induced by Con-8024 cells was 6.5-fold larger than that induced by shCHD1L-8024 cells ($P < 0.05$, paired Student's t test; Figure 7G). Increased expression of E-cadherin at cell borders and decreased expression of vimentin was observed in tumors induced by shCHD1L-8024 cells compared with those induced by Con-8024 cells (Figure 7H).

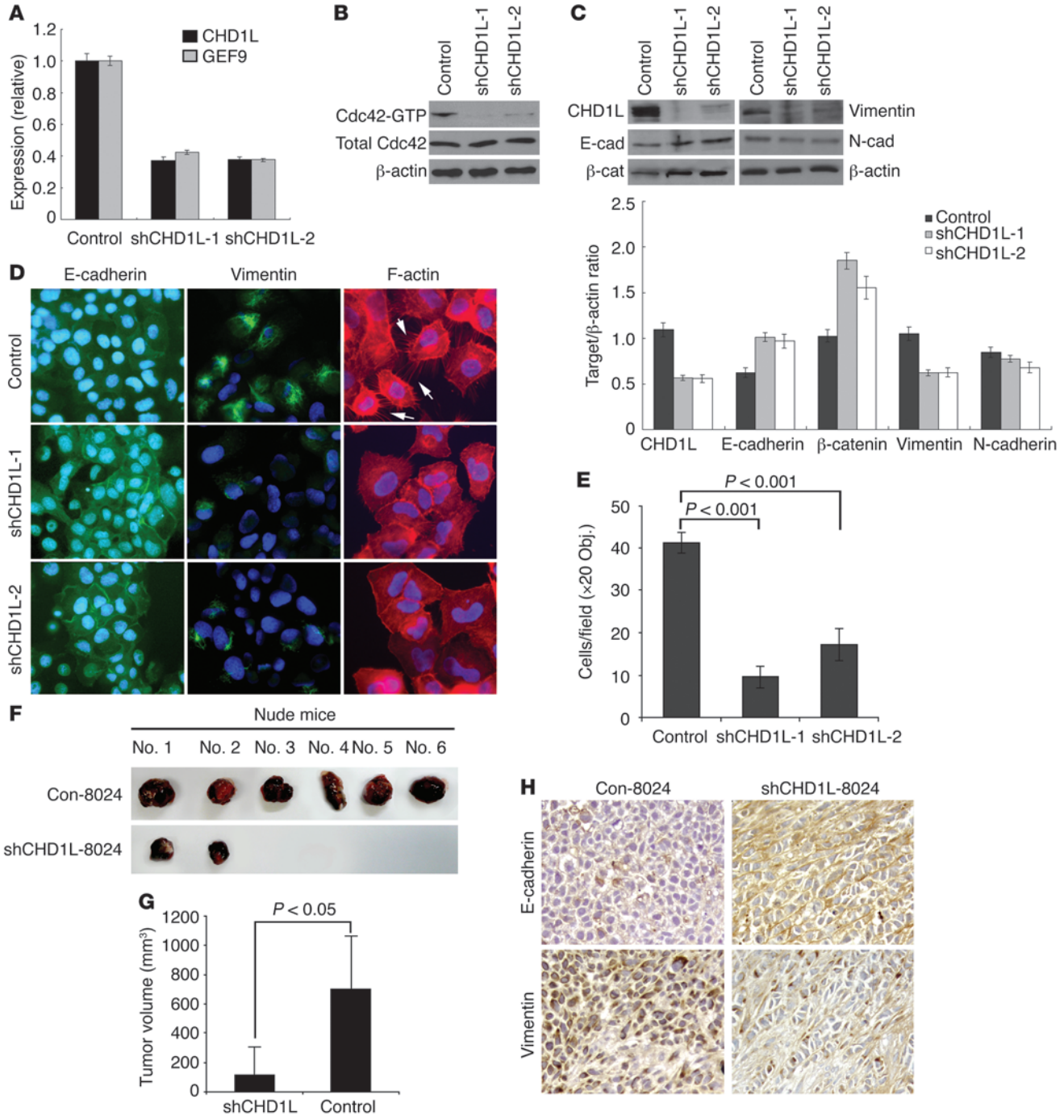

Figure 7

Silencing CHD1L expression inhibits its invasive and tumorigenic ability. (**A**) Compared with Con-8024 cells, CHD1L and ARHGEF9 expression decreased in shCHD1L-1–8024 and shCHD1L-2–8024 cells, as detected by qPCR. (**B**) Expression of Cdc42-GTP and total Cdc42 was detected by Western blot analysis. β-Actin was used as a loading control. (**C**) Expression of CHD1L, E-cadherin, β-catenin, N-cadherin, and vimentin was compared among 3 cell lines by Western blotting and quantified by densitometry (normalized to β-actin). (**D**) Representative images showing decreased formation of filopodia (arrows), increased expression of E-cadherin, and decreased expression of vimentin in shCHD1L-1–8024 and shCHD1L-2–8024 cells compared with Con-8024 cells. Nuclei were counterstained with DAPI. (**E**) Number of cells that invaded through the Matrigel was counted in 10 fields under the ×20 objective lens. (**F**) Reduced tumor volume or absent tumor formation was observed in mice injected with shCHD1L-8024 cells. (**G**) The mean volume of tumors induced by Con-8024 cells was significantly larger than that induced by shCHD1L-8024 cells on the sixth week after injection ($n = 6$). (**H**) IHC staining for E-cadherin and vimentin on serial sections of tumors induced by Con-8024 and shCHD1L-8024. Original magnification, ×400 (**D** and **H**).

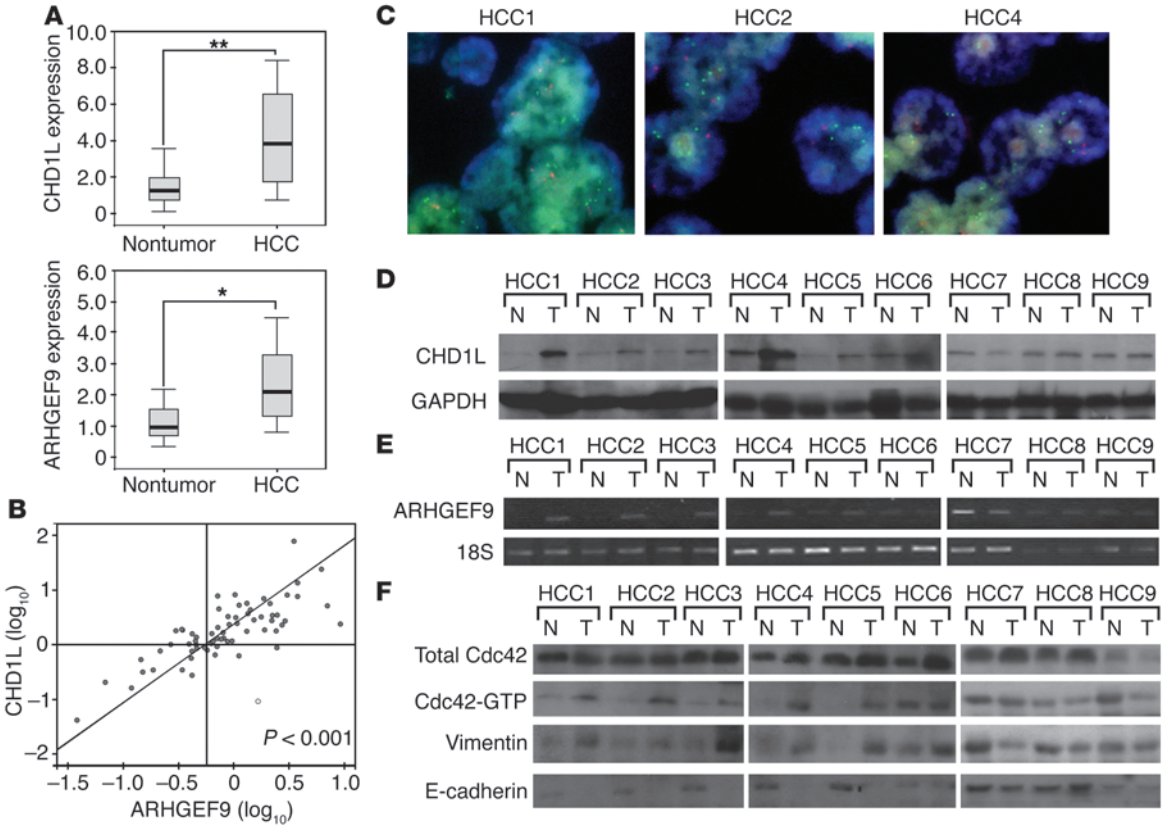

Figure 8

CHD1L overexpression correlates with ARHGEF9-meidated Cdc42 activation and EMT in human HCC. (**A**) Relative expression level of CHD1L and ARHGEF9 in 35 paired HCC and nontumor tissues, detected by qPCR. *$P < 0.05$, **$P < 0.001$, paired Student's *t* test. The boxes represent the lower and upper fold change; lines within boxes and whiskers denote mean and SD, respectively. (**B**) Correlation between CHD1L and ARHGEF9 expression in 35 paired HCCs and matched nontumor tissues, with linear regression lines and Pearson correlation significance ($P < 0.001$, Pearson χ^2 test). (**C**) Representative examples (cases HCC1, HCC2, and HCC4; see **D**) of *CHD1L* amplification in HCC specimens detected by FISH. Green signals represent BAC probe containing CHD1L gene; red signals represent centromere of chromosome 1. Original magnification, ×1,000. (**D**) Western blot analysis of CHD1L in 9 representative primary HCC tissues (T) and their paired nontumor (N) tissues. GAPDH was used as a loading control. (**E**) mRNA expression of *ARHGEF9* detected by RT-PCR. (**F**) Western blot analysis was used to determine expression levels of total Cdc42, Cdc42-GTP, vimentin, and E-cadherin in 9 representative HCCs.

All these data indicated that knockdown of CHD1L expression may abolish its invasive and tumorigenic abilities through the ARHGEF9-Cdc42-EMT pathway.

CHD1L upregulates ARHGEF9 expression in clinical HCC specimens. To further investigate whether the CHD1L-ARHGEF9 pathway is involved in HCC progression, the relationship of CHD1L overexpression with ARHGEF9 expression was tested by qPCR in 35 pairs of HCC cases. Compared with the paired nontumor tissues, overexpression (defined as greater than a 2-fold increase) of CHD1L and ARHGEF9 was detected in 20 of 35 (57.1%) and 18 of 35 (51.4%) HCCs, respectively. The average fold change of CHD1L expression in tumor tissues was significantly higher than that in paired nontumor tissues (3.85 versus 1.23; $P < 0.001$, paired Student's *t* test; Figure 8A). Similarly, the average fold change of ARHGEF9 expression in tumor tissues was significantly higher than that in their paired nontumor tissues (2.02 versus 0.91; $P < 0.05$, paired Student's *t* test; Figure 8A). Furthermore, an association study showed that ARHGEF9 expression positively correlated with CHD1L expression in these 35 pairs of HCC specimens ($r = 0.722$; $P < 0.001$, Pearson χ^2 test; Figure 8B).

The CHD1L-ARHGEF9-Cdc42 pathway promotes EMT in HCC. To further confirm the effect of the CHD1L-ARHGEF9-Cdc42 pathway on HCC progression, the correlation among *CHD1L*, *ARHGEF9*, and *Cdc42* was investigated in primary HCC specimens. Only 16 of 35 of HCCs used in the above experiment were included, selected because they had both RNA and protein samples available. To confirm the association between *CHD1L* amplification and CHD1L overexpression, FISH was used to detect DNA copy number of *CHD1L* in 9 HCC cases using a BAC probe containing *CHD1L* gene and chromosome 1 centromere probe as control. The results showed that gain of *CHD1L* copy number was detected in 5 of 9 HCC cases (HCC1–HCC5), perfectly consistent with the CHD1L overexpression in HCC1–HCC5 detected by Western blot analysis (Figure 8D). Consistent with the correlation study described above, the expression of *ARHGEF9* detected by RT-PCR also correlated closely with CHD1L expression (Figure 8E).

Next, we investigated the association among CHD1L-induced ARHGEF9 upregulation, Cdc42 activation, and the EMT phenotype in HCC cases. As shown in Figure 8F, increased expression of Cdc42-GTP, accompanied by decreased expression of E-cadherin

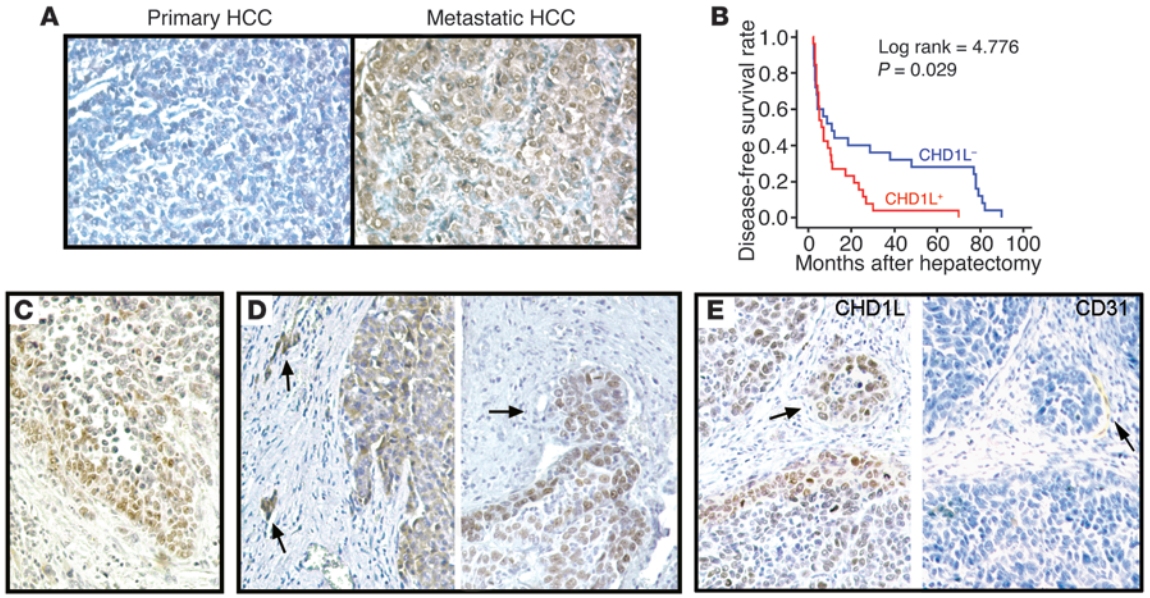

Figure 9
Overexpression of CHD1L is associated with HCC metastases and decreased DFS time. (**A**) Example of CHD1L expression detected in a primary HCC tumor and its metastatic tumor, with markedly stronger CHD1L staining in the latter. (**B**) Kaplan-Meier DFS survival curve of HCC patients in correlation with CHD1L expression. The DFS rate significantly decreased in the subgroup of HCC patients with CHD1L overexpression (red line; $n = 29$) compared with the CHD1L-negative subgroup (blue line; $n = 24$). (**C**–**E**) IHC staining with anti-CHD1L antibody showed that higher CHD1L expression was often observed in tumor cells at the tumor edge (**C**), invading (arrows) to surrounding tissue (**D**, left and right) and blood vessels (**E**, left). The endothelial cells of blood vessels were stained by IHC with an anti-CD31 antibody on the serial section of a clinical sample (**E**, right). Original magnification, ×200 (**A** and **C**–**E**).

and increased expression of vimentin, was detected in 8 of 9 (88.9%) HCC specimens with CHD1L overexpression. Conversely, increased expression of Cdc42-GTP was detected in 1 of 7 (14.3%) HCCs without CHD1L overexpression (Figure 8F). These results strongly support that the molecular pathway of CHD1L-ARHGEF9-Cdc42-EMT may play a critical role in HCC progression.

Overexpression of CHD1L is associated with HCC metastasis and poor prognosis. To investigate the correlation between CHD1L overexpression and HCC metastasis, the expression level of CHD1L was compared between primary HCCs and their paired metastatic tumors by IHC, using a tissue microarray (TMA) containing 50 pairs of primary and metastatic HCCs. Compared with their primary HCC tumors, increased expression of CHD1L was detected in 34 of 50 (68%) metastatic HCC tumors ($P < 0.001$, Wilcoxon signed rank test; Figure 9A and Supplemental Table 4). These data further support the hypothesis that CHD1L plays an important role in HCC metastasis.

To further confirm that CHD1L overexpression correlates with HCC prognosis, expression of CHD1L was examined by IHC in sections from 53 paraffin-blocked HCC specimens, with clinicopathological features including (but not limited to) tumor stage, venous metastasis, formation of microsatellite tumors, and disease-free survival (DFS) time. The results indicated that the overexpression of CHD1L was significantly associated with the presence of venous metastasis and the formation of microsatellite tumors ($P < 0.05$, Pearson χ^2 test), which is considered evidence of intrahepatic tumor metastasis (ref. 29 and Table 1). Kaplan-Meier analysis revealed that overexpression of CHD1L was significantly associated with shorter DFS rate (log-rank, 4.776; $P = 0.029$; Figure 9B). The median DFS times in the CHD1L-negative HCC patient subgroup was 11.8 months (95% confidence interval, 4.4–19.2 months; $n = 24$), and the median time in the CHD1L-positive subgroup was 6.0 months (95% confidence interval, 3.1–8.9 months; $n = 29$). Interestingly, increased expression of CHD1L was often observed in tumor cells at the edge of the tumor and in cells invading to surrounding tissue and blood vessels (Figure 9, C–E). IHC staining of CD31, a well-known vascular endothelial marker, was used to confirm the invasion of tumor cells into the blood vessel (Figure 9E, right).

Discussion

The diverse nature of the targets identified in the present study reinforces the hypothesis that CHD1L binds to and regulates diverse classes of genes that affect a wide variety of cellular processes. Genes associated with apoptosis, cell cycle, and signal transduction were relatively enriched in the CHD1L-bound loci, which is consistent with the known function of *CHD1L* (15, 16). In this study, we were particularly interested in the role of *CHD1L* in tumor cell migration, invasion, and metastasis through the upregulation of *ARHGEF9* and the subsequent activation of Rho small GTPases. Rho GTPases function as molecular switches, cycling between inactive and active GDP-bound states. Like all members of the Ras superfamily, the activity of the Rho GTPases is determined by the ratio of their GTP/GDP-bound forms in the cell (30). The ratio of the 2 forms is regulated by the opposing effects of GEFs and GTPase-activating proteins. To date, accumulating evidence has demonstrated that the majority of mammalian GEFs specific for the Rho GTPases can promote cancer cell invasion by enhancing the loading of GTP onto Rho proteins (31–34).

In the present study, we found that *CHD1L* upregulated the expression of ARHGEF9, a GEF for Cdc42, which in turn activated Cdc42 in HCC cells. Although overexpression of Cdc42 has

Table 1
Clinicopathological correlation of CHD1L expression in HCC

Feature		CHD1L protein expression		
	All	Negative	Positive	*P*
Sex				
Male	44	19	25	
Female	9	5	4	0.715
Age				
≤60 years	42	22	20	
>60 years	11	2	9	0.086
Hepatitis B surface Ag				
Negative	5	1	4	
Positive	48	23	25	0.362
Serum AFP				
log_{10} (ng/ml)	2.18 ± 1.50	2.33 ± 1.60	2.06 ± 1.45	0.543
Tumor size[A,B]				
≤5 cm	9	5	4	
>5 cm	42	18	24	0.714
Cirrhosis[A]				
Absent	16	8	8	
Present	35	16	19	1.000
Tumor encapsulation[A]				
Absent	33	15	18	
Present	17	7	10	0.506
Microsatellite formation[A]				
Absent	31	18	13	
Present	20	5	15	**0.025**
Venous invasion[A,C]				
Absent	26	16	10	
Present	24	7	17	**0.027**
Tumor stage[A,D]				
Stage I	11	8	3	
Stage II	27	11	16	
Stage III	14	5	9	0.080

Values denote *n* except for serum AFP (mean ± SD). Significant differences are shown in bold. [A]Partial data not available; statistic based on available data. [B]Measured by the length of the largest tumor nodule. [C]Defined by findings on final pathological analysis (microscopic and major). [D]American Joint Committee on Cancer classification.

been detected in breast cancer (35) and in head and neck squamous cell carcinomas (36), the role of Cdc42 in human carcinogenesis remains unclear. Increased expression of Cdc42 has been also associated with HCC. One study found that the expression of Cdc42 was higher in HBV-associated HCC tumor tissue than in adjacent nontumor liver tissues (37). Another study found that Cdc42 was overexpressed in HCV-associated HCC in comparison to normal liver (38). In this study, we revealed that the upregulation of ARHGEF9 was significantly correlated with CHD1L overexpression in clinical HCC specimens and therefore able to increase the activation of Cdc42. All these findings suggest that ARHGEF9 is a CHD1L target gene and that the molecular circuitry established by CHD1L and ARHGEF9 promotes Cdc42 activation during HCC progression.

During tumor progression, invasion, and metastasis, changes in the activity of Rho GTPase and the concomitant reorganization of the actin cytoskeleton lead to loss of the interaction of adherens junctions and the cytoskeleton (21, 23, 27, 39). Among the 20 genes encoding different members of the Rho family, Rho (RhoA, RhoB, and RhoC), Rac (Rac1, Rac2, and Rac3), and Cdc42 are 3 representative members that have been well defined for their role in modulating of the actin cytoskeleton (40). In fibroblasts and other cell types, RhoA activation induces formation of stress fibers, Rac1 stimulates lamellipodium formation, and Cdc42 induces filopodia (41). Rearrangement of the actin cytoskeleton promotes cancer progression by promoting the acquisition of migratory and invasive properties by dissociated cells, thereby allowing them to actively pass through the basement membrane and traverse to distant organs. Therefore, we hypothesized that overexpression of CHD1L may play an important role in HCC invasion and metastasis. To confirm our hypothesis, both in vitro and in vivo assays — including wound healing assays, Matrigel invasion assays, and experimental metastasis assays — were used to study whether CHD1L overexpression promotes cell motility, tumor invasion, and metastasis. Our results demonstrated that CHD1L played a key role in HCC metastasis, and further studies indicated that the overexpression of CHD1L led to increased filopodia formation and cell motility as well as EMT. Moreover, these invasion- and metastasis-associated phenotypes could be effectively abolished by silencing ARHGEF9 expression in HCC cells that overexpressed CHD1L. These findings strongly suggest that the metastatic function of CHD1L occurs through the ARHGEF9-meidated activation of Cdc42.

It has been reported that Cdc42 contributes to cancer cell invasion via the EMT (42). The EMT is a key event in tumor invasion and metastasis in which epithelial cells lose epithelial adherens and tight junction proteins, lose polarity and cell-cell contacts, and undergo remarkable remodeling of the cytoskeleton to facilitate cell motility and invasion (43, 44). The EMT includes loss of cell-cell adhesion and activation of mesenchymal markers as well as increased motility of tumor cells, which suggests that EMT is a major mechanism of tumor invasion and metastasis. To better elucidate the invasive and metastatic mechanisms of CHD1L, the effect of CHD1L overexpression or depletion on the EMT was investigated. As expected, the epithelial markers E-cadherin, α-catenin, and β-catenin were downregulated, whereas the mesenchymal markers N-cadherin, vimentin, and α-SMA were increased in CHD1L-tranfected cells. Similar results were also observed in tumors formed in nude mice induced by CHD1L-expressing cells. Further, silencing CHD1L expression in HCC cells inhibited EMT phenotype, invasive ability, and tumorigenesis in nude mice. Importantly, the EMT phenotype was also associated with overexpression of CHD1L in clinical HCC specimens. In addition, tumor invasion and tumor microsatellite formation were frequently detected in tumors induced by CHD1L-expressing cells. All of these results clearly demonstrated that the EMT induced by CHD1L is an important mechanism underlying HCC development and metastasis.

Although curative surgery offers an opportunity for a cure in HCC patients, the postoperative tumor recurrence rate is high because of a high potential for vascular invasion and metastasis, with a cumulative 5-year recurrence rate ranging from 40% to 80% (2, 45). In the present study, the invasive and metastatic effect of CHD1L in clinical specimens was also addressed by IHC in 53 HCC specimens and an HCC TMA containing 50 pairs of primary and metastatic tumors. We found that the overexpression of CHD1L was significantly correlated with the presence of tumor microsatel-

lite formation and venous metastasis in HCCs. More interestingly, the higher expression level of CHD1L was often detected in tumor cells invading into the surrounding tissue and blood vessel, which suggests that CHD1L plays an important role in tumor invasion. In addition, increased expression of CHD1L was detected in 66% of the metastatic HCC tumors compared with their paired primary HCCs. Furthermore, we also found that detection of CHD1L expression in tumor tissues could successfully distinguish a set of patients with increased risk of tumor recurrence or poor DFS rate. These findings directly demonstrate the clinical significance of CHD1L overexpression in HCC invasion and metastasis. We describe, for the first time to our knowledge, the invasive and metastatic mechanism involved in HCC progression: the transcriptional regulator CHD1L upregulates ARHGEF9 transcription, which subsequently increases Cdc42 activity, causing filopodia formation, EMT, and finally HCC invasion and metastasis.

Methods

Patients and clinical specimens. Patients who underwent hepatectomy for HCC at the Cancer Center of Sun Yat-sen University were included in the ARHGEF9 and CHD1L correlation analysis ($n = 35$) and the clinicopathological correlation analysis ($n = 53$). None of these patients received preoperative chemotherapy or radiotherapy. All tumor samples were derived from dissected tumor tissues and were composed of more than 90% of tumor cells without necrosis. The surgical specimens (both tumor and adjacent nontumor tissue) were processed immediately after the operation and snap-frozen in liquid nitrogen (for protein, DNA, and RNA extraction) and/or embedded in paraffin block (for pathological study). All HCC patients gave written informed consent on the use of clinical specimens for medical research. Studies using human tissue were reviewed and approved by the Committees for Ethical Review of Research involving Human Subjects of Zhongshan University (Guangzhou, China) and University of Hong Kong.

Cell lines and culture conditions. The HCC cell lines QGY-7703 and PLC8024 and an immortalized normal human liver cell line, LO-2, were obtained from the Institute of Virology, Chinese Academy of Medical Sciences (Beijing). The cells were maintained in high-glucose DMEM (Invitrogen) supplemented with 10% fetal calf serum (Invitrogen). The cells were incubated at 37°C in a humidified chamber containing 5% CO_2.

Plasmid constructs and transfection. The full-length CHD1L cDNA was amplified and cloned into the pCDNA3.1$^+$ expression vector (Invitrogen) as described previously (15). pEGFP-CHD1L was generated by inserting the cloned full-length CHD1L into pEGFP-N1 vector (Invitrogen) as described previously (16). The expression plasmids were transfected into cells using Lipofectamine 2000 (Invitrogen) according to the manufacturer's instructions.

Establishment of CHD1L knockdown cells. Based on the *CHD1L* sequence (NM_004284), 2 shRNAs were designed using siRNA Target Finder (Ambion): shCHD1L-1, 5′-GCCAAGAGAAGGAGA-3′; shCHD1L-2, 5′-CGTATTGGACATGCCACGAAA-3′. The oligoduplexes were cloned into the pRetroSuper (pRS) vector (Origene) or control pRS vector and transfected into PLC8024 cells using Lipofectamine 2000 (Invitrogen). At 24 hours after transfection, transfected cells were selected for 2 weeks with 1 μg/ml puromycin (Origene). Pooled populations of knockdown cells, obtained 2 weeks after drug selection without subcloning, were subjected in both in vivo and in vitro experiments. Negative control cell lines were generated by infecting cells with pRS-shGFP construct targeting GFP cDNA (Origene), a purified and sequence-verified plasmid containing a noneffective 29-mer shGFP cassette.

Antibodies. Mouse anti-CHD1L antibody was purchased from Abcam. Rabbit anti–N-cadherin, –β-catenin, and –α-catenin antibodies were purchased as part of the Cadherin-Catenin Antibody Sampler Kit (Cell Signalling Technology). Mouse anti-vimentin, –E-cadherin, –α-SMA, –β-actin, and -GAPDH antibodies were purchased from Santa Cruz Biotechnology. Mouse anti–E-cadherin antibody (ready to use for IHC) was purchased from Genway Biotech Inc. Rabbit anti-CD31 antibody was purchased from Boster.

ChIP cloning. ChIP experiments were performed using an EZ-Magna ChIP G kit (Upstate Biotechnology) according to the manufacturer's instructions. To facilitate cloning of the immunoprecipitated DNA fragments, the purified DNA fragments were linked with an adaptor using primer A [GTTTCCCAGTCACGGTC(N)$_9$] and random priming. The immunoprecipitated DNA fragments with adaptors were then amplified using the adaptor primer B [GTTTCCCAGTCACGGTC] and PCR. The enriched DNA fragments (about 200–400 bp) were purified with a PCR Purification Kit (Qiagen), cloned into the pGEM-T easy vector (Promega), and sequenced.

EMSA. Nuclear extracts (NEs) were prepared using the NucBuster Protein Extraction kit (Novagen). The probes were end-labeled with DIG by PCR using DIG-labeled dUTP (Roche) in addition to dNTPs. The probes were then purified by a PCR Purification Kit (Qiagen). EMSAs were performed with 10 μg NEs and 50 ng DIG-labeled or unlabeled probes in 1× binding buffer provided with the Bandshift Kit (Amersham Pharmacia Biotech). This binding reaction was separated on a nondenaturing polyacrylamide gel and transferred to a nylon membrane (Amersham Pharmacia Biotech). The resolved complexes were crosslinked using an UV crosslinker oven for 3 minutes. The shifted bands corresponding to the protein-DNA complexes were detected using a DIG Luminescent Detection Kit (Roche) and visualized using BioMax Light film (Kodak).

ChIP-PCR. The identified CHD1L binding sites were confirmed using independent ChIP-PCR assays with immunoprecipitated DNA fragments pulled down by anti-GFP antibodies FL and B-2, or pooled IgG from mouse and rabbit (Santa Cruz Biotechnology) as a negative control. The primers used for the amplification of the precipitated DNA fragments are listed in Supplemental Table 5.

qPCR. Total RNA was extracted using TRIzol Reagent (Invitrogen), and reverse transcription was performed using an Advantage RT-for-PCR Kit (Clontech Laboratories) according the manufacturer's instructions. For qPCR analysis, aliquots of double-stranded cDNA were amplified using a SYBR Green PCR Kit (Applied Biosystems) and an ABI PRISM 7900 Sequence Detector. The cycling parameters were 95°C for 30 seconds, 55°C for 1 minute, and 72°C for 2 minutes for 45 cycles, followed by a melting curve analysis. Ct was measured during the exponential amplification phase, and the amplification plots were analyzed using SDS 1.9.1 software (Applied Biosystems). For the cell lines, the relative expression level (defined as fold change) of target gene is given by $2^{-\Delta\Delta Ct}$ ($\Delta Ct = \Delta Ct^{target} - \Delta Ct^{18S}$; $\Delta\Delta Ct = \Delta Ct^{\text{CHD1L-expressing or siCHD1L-8024}} - \Delta Ct^{\text{vector-transfected or Con-8024}}$) and normalized to the fold change detected in the corresponding control cells, which was defined as 1.0. For clinical HCCs and their matched nontumor specimens, the fold change of target gene is given by $2^{-\Delta\Delta Ct}$ ($\Delta\Delta Ct = \Delta Ct^{tumor} - \Delta Ct^{nontumor}$) and normalized to the average fold change in 35 nontumor tissues, which was defined as 1.0. All reactions were performed in duplicate. Primer sequences are listed in Supplemental Table 6.

RNAi. An siRNA (20 nM) against CHD1L, ARHGEF9, or GAPDH (Ambion) was transfected into cells in 6-well plates using Lipofectamine 2000 (Invitrogen) according to the manufacturer's instructions. Gene silencing was measured by qPCR and/or Western blot analysis 48 hours after transfection.

FISH. A BAC clone at 1q21 containing the *CHD1L* gene (RP11-337C18) was selected for interphase FISH study. BAC DNA and probe for chromosome 1 centromere were labeled with Spectrum-green (green signal) and Spectrum-red (red signal), respectively (Vysis). FISH reaction was performed according to the method described previously (46).

Western blot. Western blot analysis was performed as described previously (15). Signals were quantified by ImageJ software (http://rsb.info.nih.gov/ij) and defined as the ratio of target protein to β-actin. Data are presented as mean ± SD (n = 3).

Rho GTPase activation assay. This assay was performed using a Rac1/Cdc42 Activation Kit (Upstate Biotechnology). The PAK1-P21-binding domain agarose beads provided in this kit were used to pull down Cdc42-GTP from whole cell lysates according to the manufacturer's instructions. Cdc42-GTP was then detected by Western blot using the Cdc42 monoclonal antibody provided in the kit.

F-actin and IF staining. After fixation with 4% paraformaldehyde in PBS for 10 minutes, the cells were washed twice with PBS. For F-actin staining, cells were stained with Rhodamine phalloidin (Invitrogen). For IF staining, cells were incubated with the primary antibody (mouse anti–E-cadherin, -vimentin, or –N-cadherin or rabbit anti–β-catenin; 1:100 dilution) overnight at 4°C. After thorough washing, cells were then incubated with FITC-conjugated goat anti-mouse IgG (1:100 dilution, Santa Cruz Biotechnology) or Texas Red–conjugated goat anti-rabbit IgG (1:100 dilution, Santa Cruz Biotechnology). Finally, cells were washed and mounted with Mounting Medium containing DAPI (Vector Laboratories). Images were captured using a Leica DMRA fluorescence microscope (Rueil-Malmaison).

Wound healing and invasion assays. Cell migration was assessed by measuring the movement of cells into a scraped, acellular area created by a 200-μl pipette tube, and the spread of wound closure was observed after 24 and 36 hours and photographed under a microscope. Invasion assays were performed with 24-well BioCoat Matrigel Invasion Chambers (BD) according to the manufacturer's instructions. The number of cells that invaded through the Matrigel was counted in 10 fields under a ×20 objective lens.

Tumor xenograft mouse model. Female athymic nude mice (4–5 weeks old) were housed under standard conditions and cared for according to the institutional guidelines for animal care. All animal experiments were approved by the Committee on the Use of Live Animals in Teaching and Research (CULATR), University of Hong Kong. For the xenograft tumor growth assay, control cells (Vec-LO2, Vec-7703, and Con-8024) were injected subcutaneously into the left dorsal flank of mice, and CHD1L-expressing or knockdown cells (CHD1L-LO2, CHD1L-7703, and shCHD1L-8024) were injected into the right dorsal flank of the same animal in a laminar flow cabinet. Tumor formation in nude mice was monitored over a 4-week period, and the tumor volume was measured weekly and calculated as $0.5 \times l \times w^2$ (47). The mice were euthanized on the fifth or sixth week, and the tumors were excised and embedded in paraffin. Sections (5 μm) of tumors were stained with H&E to visualize the tumor structure.

Experimental metastasis assay. Male SCID-Beige mice (5 weeks old) were used, and each experimental group (Vec-7703 and CHD1L-7703) consisted of 6 mice. Briefly, 2×10^5 cells were injected intravenously through the tail vein into each SCID mouse. All mice were euthanized 8 weeks after injection. The presence of tumor nodules was macroscopically determined, and the number of tumor nodules formed on the lung and liver surfaces was counted. The livers and lungs were excised and embedded in paraffin. All animal procedures were performed in full accordance with a CULATR-approved protocol.

TMA construction. A TMA block containing primary and matched metastatic HCCs was constructed as described previously (48). TMA contained 50 pairs of primary HCCs and their matched metastatic tumors from the same patients. These tumor samples were collected from archives of paraffin-embedded tissues obtained between 1997 and 2003 at the Department of Pathology, Sun Yat-sen University. Metastatic tumors included 28 intrahepatic metastases (23 portal vein, 5 cholangiotube) and 22 extrahepatic metastases (16 peritoneum, 5 lymph nodes, 1 kidney). Multiple sections (5 μm thick) were cut from the TMA block and mounted on microscope slides.

IHC. The paraffin-embedded tissue blocks were sectioned for IHC. In brief, sections were deparaffinized and rehydrated. The endogenous peroxidase activity was blocked with 3% H_2O_2 for 10 minutes. For the antigen retrieval, slides were immersed in 10 mM citrate buffer (pH 6.0) and boiled for 15 minutes in a microwave oven. Nonspecific binding was blocked by 5% normal goat serum for 10 minutes. The slides were incubated with a 1:50 dilution of monoclonal antibody against CHD1L (Abcam) at 4°C overnight in a moist chamber. The slides were sequentially incubated with biotinylated goat anti-mouse IgG (1:100 dilution; Santa Cruz Biotechnology) and then streptavidin-peroxidase conjugate, each for 30 minutes at room temperature. Isotope-matched human IgG was used in each case as a negative control. Finally, the 3, 5-diaminobenzidine (DAB) Substrate Kit (Dako) was used for color development followed by Mayer hematoxylin counterstaining.

Statistics. Unless otherwise indicated, data are presented as mean ± SD of 3 independent experiments. The SPSS statistical package for Windows (version 16; SPSS) was used for data analysis. Based on staining intensities, the CHD1L immunoreactivity was scored as negative (0 to 1) and positive (2 to 3) according to a previously reported semiquantitative scoring method (49). The clinicopathological features in CHD1L-positive and -negative patients were compared using Pearson χ^2 test for categorical variables and independent Student's t test for continuous data. Kaplan-Meier plots and log-rank tests were used for survival analysis. DFS times were calculated from data of curative surgery to HCC recurrence, death, or the last follow-up data. For TMA analysis, based on IHC scores, CHD1L protein levels in primary HCC tissues and their matched metastatic tissues were compared using Wilcoxon signed rank test. The mRNA level of CHD1L and ARHGEF9 in the HCCs and the matched nontumor tissue was compared using paired Student's t test. The correlation between mRNA levels of CHD1L and ARHGEF9 was analyzed using Pearson χ^2 test. The independent Student's t test was used to compare the invasive ability between any 2 preselected groups. A P value less than 0.05 was considered statistically significant.

Acknowledgments

This work was supported by a Hong Kong Research Grant Council Grant (HKU 7656/07M), Hong Kong Research Grant Council Central Allocations (HKU 1/06C and HKU5/CRF/08), the "Hundred Talents Program" at Sun Yat-sen University (85000-3171311), the Major State Basic Research Program of China (2006CB910104), and a grant from the National Natural Science Foundation of China (30772475).

Received for publication August 2, 2009, and accepted in revised form January 13, 2010.

Address correspondence to: Xin-Yuan Guan, Department of Clinical Oncology, University of Hong Kong, Room L10-56, Laboratory Block, 21 Sassoon Road, Hong Kong, China. Phone: 852.28199782; Fax: 852.28169126; E-mail: xyguan@hkucc.hku.hk.

1. Thorgeirsson SS, Grisham JW. Molecular pathogenesis of human hepatocellular carcinoma. *Nat Genet*. 2002;31(4):339–346.
2. Tung-Ping Poon R, Fan ST, Wong J. Risk factors, prevention, and management of postoperative recurrence after resection of hepatocellular carcinoma. *Ann Surg*. 2000;232(1):10–24.
3. Fidler IJ. The pathogenesis of cancer metastasis: the 'seed and soil' hypothesis revisited. *Nat Rev Cancer*. 2003;3(6):453–458.
4. Tsuda H,et al. Allele loss on chromosome 16 associated with progression of human hepatocellular carcinoma. *Proc Natl Acad Sci U S A*. 1990;87(17):6791–6794.
5. Qin LX, et al. The association of chromosome 8p deletion and tumor metastasis in human hepatocellular carcinoma. *Cancer Res*. 1999;59(22):5662–5665.
6. Chuma M, et al. Overexpression of cortactin is

involved in motility and metastasis of hepatocellular carcinoma. *J Hepatol*. 2004;41(4):629–636.
7. Lau S H, et al. Clusterin plays an important role in hepatocellular carcinoma metastasis. *Oncogene*. 2006;25(8):1242–1250.
8. Wu X, et al. HTPAP gene on chromosome 8p is a candidate metastasis suppressor for human hepatocellular carcinoma. *Oncogene*. 2006;25(12):1832–1840.
9. Lee TK, et al. Twist overexpression correlates with hepatocellular carcinoma metastasis through induction of epithelial-mesenchymal transition. *Clin Cancer Res*. 2006;12(18):5369–5376.
10. Sun CK, et al. The significance of proline-rich tyrosine kinase2 (Pyk2) on hepatocellular carcinoma progression and recurrence. *Br J Cancer*. 2007;97(1):50–57.
11. Marchio A, et al. Recurrent chromosomal abnormalities in hepatocellular carcinoma detected by comparative genomic hybridization. *Genes Chromosomes Cancer*. 1997;18(1):59–65.
12. Wong N, et al. Assessment of genetic changes in hepatocellular carcinoma by comparative genomic hybridization analysis: relationship to disease stage, tumor size, and cirrhosis. *Am J Pathol*. 1999;154(1):37–43.
13. Guan XY, et al. Recurrent chromosome alterations in hepatocellular carcinoma detected by comparative genomic hybridization. *Genes Chromosomes Cancer*. 2000;29(2):110–116.
14. Wong N, et al. Positional mapping for amplified DNA sequences on 1q21-q22 in hepatocellular carcinoma indicates candidate genes over-expression. *J Hepatol*. 2003;38(3):298–306.
15. Ma NF, et al. Isolation and characterization of a novel oncogene, amplified in liver cancer 1, within a commonly amplified region at 1q21 in hepatocellular carcinoma. *Hepatology*. 2008;47(2):503–510.
16. Chen L, et al. Chromodomain helicase/adenosine triphosphatase DNA binding protein 1-like (CHD1L) gene suppresses the nucleus-to-mitochondria translocation of nur77 to sustain hepatocellular carcinoma cell survival. *Hepatology*. 2009;50(1):122–129.
17. Eisen JA, Sweder KS, Hanawalt PC. Evolution of the SNF2 family of proteins: subfamilies with distinct sequences and functions. *Nucleic Acids Res*. 1995;23(14):2715–2723.
18. Pazin MJ, Kadonaga JT. SWI2/SNF2 and related proteins: ATP-driven motors that disrupt protein-DNA interactions? *Cell*. 1997;88(6):737–740.
19. Woodage T, et al. Characterization of the CHD family of proteins. *Proc Natl Acad Sci U S A*. 1997;94(21):11472–11477.
20. Hug BA, et al. A chromatin immunoprecipitation screen reveals protein kinase Cbeta as a direct RUNX1 target gene. *J Biol Chem*. 2004;279(2):825–830.
21. Noren NK, et al. p120 catenin regulates the actin cytoskeleton via Rho family GTPases. *J Cell Biol*. 2000;150(3):567–580.
22. Braga VM. Cell-cell adhesion and signalling. *Curr Opin Cell Biol*. 2002;14(5):546–556.
23. Sahai E, Marshall CJ. RHO-GTPases and cancer. *Nat Rev Cancer*. 2002;2(2):133–142.
24. Cartharius K, et al. MatInspector and beyond: promoter analysis based on transcription factor binding sites. *Bioinformatics*. 2005;21(13):2933–2942.
25. Chilton BS, Hewetson A. Progesterone regulation of RUSH/SMARCA3/HLTF includes DNA looping. *Biochem Soc Trans*. 2008;36(Pt 4):632–636.
26. Reid T, et al. Identification and characterization of hPEM-2, a guanine nucleotide exchange factor specific for Cdc42. *J Biol Chem*. 1999; 274(47):33587–33593.
27. Hall A. Rho GTPases and the control of cell behaviour. *Biochem Soc Trans*. 2005;33(Pt 5):891–895.
28. Thiery JP, Sleeman JP. Complex networks orchestrate epithelial-mesenchymal transitions. *Nat Rev Mol Cell Biol*. 2006;7(2):131–142.
29. Ho MK, et al. Allelic alterations in nontumorous liver tissues and corresponding hepatocellular carcinomas from chinese patients. *Hum Pathol*. 2003;34(7):699–705.
30. Boguski MS, McCormick F. Proteins regulating Ras and its relatives. *Nature*. 1993;366(6456):643–654.
31. Habets GG, et al. Identification of an invasion-inducing gene, Tiam-1, that encodes a protein with homology to GDP-GTP exchangers for Rho-like proteins. *Cell*. 1994;77(4):537–549.
32. Van Aelst L, D'Souza-Schorey C. Rho GTPases and signaling networks. *Genes Dev*. 1997; 11(18):2295–2322.
33. Adam L, et al. Tiam1 overexpression potentiates heregulin-induced lymphoid enhancer factor-1/beta -catenin nuclear signaling in breast cancer cells by modulating the intercellular stability. *J Biol Chem*. 2001;276(30):28443–28450.
34. Vega FM, Ridley AJ. Rho GTPases in cancer cell biology. *FEBS Lett*. 2008;582(14):2093–2101.
35. Fritz G, Brachetti C, Bahlmann F, Schmidt M, Kaina B. Rho GTPases in human breast tumours: expression and mutation analyses and correlation with clinical parameters. *Br J Cancer*. 2002;87(6):635–644.
36. Abraham MT, Kuriakose MA, Sacks PG, Yee H, Chiriboga L, Bearer EL, Delacure MD. Motility-related proteins as markers for head and neck squamous cell cancer. *Laryngoscope*. 2001;111(7):1285–1289.
37. Chang CS, Huang SM, Lin HH, Wu CC, Wang CJ. Different expression of apoptotic proteins between HBV-infected and non-HBV-infected hepatocellular carcinoma. *Hepatogastroenterology*. 2007;54(79):2061–2068.
38. Cooper AB, Wu J, Lu D, Maluccio MA. Is autotaxin (ENPP2) the link between hepatitis C and hepatocellular cancer? *J Gastrointest Surg*. 2007;11(12):1628–1634; discussion 1634–1635.
39. Wicki A, et al. Tumor invasion in the absence of epithelial-mesenchymal transition: podoplanin-mediated remodeling of the actin cytoskeleton. *Cancer Cell*. 2006;9(4):261–272.
40. Lozano E, Betson M, Braga VM. Tumor progression: Small GTPases and loss of cell-cell adhesion. *Bioessays*. 2003;25(5):452–463.
41. Hall A. Rho GTPases and the actin cytoskeleton. *Science*. 1998;279(5350):509–514.
42. Friedl P, Wolf K. Tumour-cell invasion and migration: diversity and escape mechanisms. *Nat Rev Cancer*. 2003;3(5):362–374.
43. Thiery JP. Epithelial-mesenchymal transitions in tumour progression. *Nat Rev Cancer*. 2002;2(6):442–454.
44. Kang Y, Massague J. Epithelial-mesenchymal transitions: twist in development and metastasis. *Cell*. 2004;118(3):277–279.
45. Chang CH, et al. Long-term results of hepatic resection for hepatocellular carcinoma originating from the noncirrhotic liver. *Arch Surg*. 2004;139(3):320–325; discussion 326.
46. Guan XY, Sham JS, Tang TC, Fang Y, Huo KK, Yang JM. Isolation of a novel candidate oncogene within a frequently amplified region at 3q26 in ovarian cancer. *Cancer Res*. 2001;61(9):3806–3809.
47. Cao Z A, Daniel D, Hanahan D. Sub-lethal radiation enhances anti-tumor immunotherapy in a transgenic mouse model of pancreatic cancer. *BMC Cancer*. 2002;3:11.
48. Wang Y, et al. Prognostic significance of c-myc and AIB1 amplification in hepatocellular carcinoma. A broad survey using high-throughput tissue microarray. *Cancer*. 2002;95(11):2346–2352.
49. Ng IO, et al. Overexpression and point mutations of p53 tumor suppressor gene in hepatocellular carcinomas in Hong Kong Chinese people. *Cancer*. 1994;74(1):30–37.